Pergamon

Int. J. Solids Structures Vol. 33, No. 11, pp. 1543–1562, 1996

0020-7683/96 $15.00 + .00

0020-7683(95)00118-2

FAST TRANSIENT DYNAMIC PLANE STRESS ANALYSIS OF ORTHOTROPIC HILL-TYPE SOLIDS AT FINITE ELASTOPLASTIC STRAINS

PAUL STEINMANN, CHRISTIAN MIEHE and ERWIN STEIN
Institut für Baumechanik und Numerische Mechanik Universität Hannover, Appelstrs. 9a, Germany

(*Received* 23 *February* 1995; *in revised form* 18 *May* 1995)

Abstract—The objective of this work is the geometrically nonlinear plane stress analysis of orthotropic Hill type elastoplastic solids under short term dynamic loading conditions. Thereby, the underlying motivation is the necessity to model the anisotropic behaviour of metal specimens which is due to the manufacturing procedure in terms of an orthotropic yield condition. To this end, the classical von Mises condition in the framework of multiplicative elastoplasticity is substituted by a yield criterion which invokes a second order anisotropy tensor acting on the deviatoric stresses in the plastic intermediate configuration. A reparametrization of this model reveals its relation to the classical criterion originally proposed by Hill in the geometrically linear setting. Moreover an element technology is outlined recovering the plane stress response of arbitrary 3D constitutive models without any plane stress specific modifications in the large strain regime. The intriguing influence of certain types of orthotropy on the failure patterns of thin metal sheets under plane stress uniaxial extension is investigated numerically. Thereby, an explicit time stepping procedure designed to incorporate the developed plane stress element is employed to trace the short term response predictions of the investigated specimens.

1. INTRODUCTION

The strength properties of a wide variety of engineering materials exhibit anisotropic behaviour. Consider as a paradigm thin metal sheets where the anisotropy is induced by the manufacturing process in the form of crystallographic texture. This kind of anisotropy can be modelled with good accuracy by the assumption of an orthotropic loading function within an elastoplastic constitutive description. In experiments the elastoplastic behaviour of metals is almost independent of the hydrostatic pressure thus allowing expression of an orthotropic yield criterion in terms of the deviatoric stresses. The classical pressure independent extension of the isotropic von Mises approach to capture orthotropic strength properties has been formulated by Hill (1948) within a geometrically linear setting.

The objective of this work is to formulate an orthotropic yield condition within the framework of large strain multiplicative elastoplasticity. Thereby, the constitutive relations are derived with reference to the plastic intermediate configuration which is assumed to be isoclinic. Following the traditional lines advocated by Boehler (1987) we establish an orthotropic yield condition as an isotropic function of a stress measure in the intermediate configuration which was originally proposed by Mandel (1972) and a set of structural tensors describing the prefered axes of the material. The actual choice of the invariants in the yield condition is motivated by simple arguments. We combine the orthotropic yield condition with an isotropic hyperelastic free energy function in order to concentrate exclusively on the effects induced by the orthotropic loading function.

The resulting evolution equations for the plastic deformation gradient are then integrated implicitly with the plastic volume preserving exponential map integrator. Thereby, the algorithmic flow direction is symmetric due to the restriction to an isotropic elastic response thus simplifying the evaluation of the tensor exponent. The iteration operator for the local integration algorithm is discussed in detail.

On the finite element level, the objective is to extend an element technology developed in Steinmann *et al.* (1995) recovering the plane stress response of 3D constitutive models without any plane stress specific modifications to the dynamic case. Thereby, the central

idea of the present formulation is to split the three dimensional solution domain into the plane midsurface and the out-of-plane domain and subsequently parametrize the out of plane deformation in the node point thickness. As a consequence it is indeed possible to show that for thin elements the plane stress constraint is satisfied in the weak sense with the variation of the thickness as a weighting function.

In catastrophic loading cases, or in metal forming, high speed deformations of thin metal sheets are very likely to occur. Our interest is therefore to simulate the short term response to these loading cases by an explicit solution strategy tracing the dynamic deformation behaviour. To this end we briefly describe an explicit time stepping algorithm designed to handle the plane stress element described above. The necessity to incorporate 3D constitutive models in order to describe realistically ductile failure mechanisms in an explicit dynamic setting was recently pointed out by Mathur *et al.* (1994).

Besides the usual measurements of strength properties the observation of the failure behaviour plays an essential role in the realistic description of materials. Therefore, it is the main aim of the numerical example to examine the influence of orthotropy in the yield strength on the resulting failure patterns of thin metal sheets under plane stress extension. Typically, failure at the constitutive level may result in a spatial discontinuity of the velocity gradient field which manifests itself in localization of inelastic deformations into narrow bands. These bands act as a precursor to subsequent fracturing which is not addressed in this work. An analytical localization analysis has been carried out in Steinmann *et al.* (1993) for the geometrically linear case. The essential outcome of the present numerical study is to demonstrate the intriguing influence of an orthotropic yield condition on the spatial orientation of localized failure modes under the plane stress constraint in the large strain regime. Thereby, extreme cases for uniaxial extension loading are on the one hand a splitting failure type mode, typical for brittle materials, and on the other hand the classical ductile shear banding mode which is well known from plane strain calculations incorporating the isotropic von Mises model.

2. CONTINUUM MECHANICS FRAMEWORK

To set the stage we briefly review the essential features of finite multiplicative elastoplasticity. For later use it proves convenient to emphasize from the onset issues of covariant and contravariant tensor field representations. The advantage of a mixed variant setting of multiplicative elastoplasticity has been pointed out by Miehe (1994) and Miehe and Stein (1992). In the following, we indicate covariant and contravariant tensor fields by $(\bullet)^\flat$ and $(\bullet)^\#$, all other tensor fields are mixed variant.

Assume the nonlinear deformation map $\mathbf{x} = \boldsymbol{\varphi}(\mathbf{X}, t) : \mathscr{B}_0 \times \mathscr{I} \to \mathbb{R}^3$ mapping particles labeled with $\mathbf{X}$ in the reference configuration to their actual position $\mathbf{x}$ in the deformed configuration $\mathscr{B}$ within the time interval $\mathscr{I}$. Then $\mathbf{F} = \nabla_{\mathbf{X}}\boldsymbol{\varphi}$ with Jacobi determinant $J = \det \mathbf{F} > 0$ denoting the deformation gradient with local multiplicative decomposition $\mathbf{F} = \mathbf{F}_e \cdot \mathbf{F}_p$ into an elastic $\mathbf{F}_e$ and a plastic part $\mathbf{F}_p$ see Lee (1969). The contra-covariant spatial velocity gradient is denoted by $\mathbf{l} = \dot{\mathbf{F}} \cdot \mathbf{F}^{-1}$ and decomposes additively

$$\mathbf{l} = \dot{\mathbf{F}}_e \cdot \mathbf{F}_e^{-1} + \mathbf{F}_e \cdot \dot{\mathbf{F}}_p \cdot \mathbf{F}_p^{-1} \cdot \mathbf{F}_e^{-1} = \mathbf{l}_e + \mathbf{F}_e \cdot \mathbf{L}_p \cdot \mathbf{F}_e^{-1} = \mathbf{l}_e + \mathbf{l}_p. \tag{1}$$

The elastoplastic decomposition introduces the notion of the plastic intermediate configuration $\mathscr{B}_p$ assumed as macro stress free. Then we can define a set of strain measures associated with the multiplicative decomposition. Among them the most important one for the subsequent derivations is the covariant elastic right Cauchy–Green tensor $\mathbf{C}_e^\flat$ defined in the intermediate configuration $\mathscr{B}_p$

$$\mathbf{C}_e^\flat = \mathbf{F}_e^t \cdot \mathbf{F}_e. \tag{2}$$

Geometrically, this fundamental strain measure is connected via elastic or plastic pull-back

and push-forward with the covariant spatial metric $\mathbf{g}^\flat$ and the covariant right Cauchy–Green tensor, respectively

$$\mathbf{C}_e^\flat = \mathbf{F}_e^t \cdot \mathbf{g}^\flat \cdot \mathbf{F}_e = \mathbf{F}_p^{-t} \cdot \mathbf{C}^\flat \cdot \mathbf{F}_p^{-1}. \tag{3}$$

Guided by this consideration, the reduced form of the Clausius–Duhem inequality is expressed either in terms of the contravariant Kirchhoff stress $\boldsymbol{\tau}^\#$ in $\mathscr{B}$ and the covariant rate of deformation tensor $\mathbf{l}^{sym} = \frac{1}{2}\mathscr{L}_v(\mathbf{g}^\flat)$, the contravariant second Piola–Kirchhoff stress $\boldsymbol{\Sigma}_p^\#$ in $\mathscr{B}_p$ and covariant plastic Lie derivative of the elastic right Cauchy–Green tensor $\mathscr{L}_v^p(\mathbf{C}_e^\flat)$ or the contravariant second Piola–Kirchhoff stress $\boldsymbol{\Sigma}_2^\#$ in $\mathscr{B}_0$ and rate of the covariant right Cauchy–Green tensor $\dot{\mathbf{C}}^\flat$

$$\tfrac{1}{2}\boldsymbol{\tau}_p^\# : \mathscr{L}_v(\mathbf{g}^\flat) - \dot{\Psi} = \tfrac{1}{2}\boldsymbol{\Sigma}_p^\# : \mathscr{L}_v^p(\mathbf{C}_e^\flat) - \dot{\Psi} = \tfrac{1}{2}\boldsymbol{\Sigma}_2^\# : \dot{\mathbf{C}}^\flat - \dot{\Psi} \geqslant 0. \tag{4}$$

Due to the restrictions of the principle of material frame indifference the macro part of the Helmholtz free energy Ψ^{mac} is formulated most generally in terms of the elastic right Cauchy–Green tensor $\mathbf{C}_e^\flat$. For an account on this argument refer e.g. to Miehe and Stein (1992) or Miehe *et al.* (1994). An additional scalar internal variable q is responsible for isotropic hardening and is the argument of the micro part of the Helmholtz free energy Ψ^{mic}

$$\Psi = \Psi^{mac}(\mathbf{C}_e^\flat) + \Psi^{mic}(q). \tag{5}$$

Taking into account the definition of the plastic Lie derivative of the elastic right Cauchy–Green tensor

$$\mathscr{L}_v^p(\mathbf{C}_e^\flat) = \mathbf{F}_p^{-t} \cdot \dot{\mathbf{C}}^\flat \cdot \mathbf{F}_p^{-1} = \dot{\mathbf{C}}_e^\flat + 2[\mathbf{C}_e^\flat \cdot \mathbf{L}_p]^{sym} \tag{6}$$

the hyperelastic constitutive law, the isotropic hardening law and the remaining dissipation inequality follow as

$$\boldsymbol{\Sigma}_p^\# = 2\frac{\partial \psi^{mac}}{\partial \mathbf{C}_e^\flat} \quad \text{and} \quad p =: \frac{\partial \psi^{mic}}{\partial q} \quad \text{and} \quad D = \mathbf{S} : \mathbf{L}_p - p\dot{q} \geqslant 0 \quad \text{with} \quad \mathbf{S} = \mathbf{C}_e^\flat \cdot \boldsymbol{\Sigma}_p^\# \tag{7}$$

The stress tensor $\mathbf{S}$, which was originally introduced by Mandel (1972), has been given a mixed-variant, i.e. co-contravariant, interpretation by Miehe (1994). It is only symmetric if the hyperelastic constitutive law is isotropic. Next, the framework of an associated structure for multiplicative plasticity is suggested by the principle of maximum dissipation, see Hill (1950) or Lubliner (1984), with Φ the yield condition

$$-D(\mathbf{S}, h) + \gamma\Phi(\mathbf{S}, p) \to \text{stat.} \tag{8}$$

The principle of maximum dissipation renders the associated flow rule for the plastic velocity gradient on $\mathscr{B}_p$ and the associated evolution law for the hardening variable q, please refer as well to the early work by Mandel (1972), Lubliner (1986) or Miehe and Stein (1992) and references therein

$$\mathbf{L}_p = \gamma\, \partial_S\Phi \quad \text{and} \quad \dot{q} = -\gamma\, \partial_p\Phi. \tag{9}$$

A spatial format of multiplicative associative elastoplasticity taking into account the isotropy of the elastic and the plastic response was outlined by Simo and Miehe (1992).

3. ISOTROPIC FREE ENERGY FUNCTION

For the macro part of the Helmholtz free energy Ψ^{mac} we restrict ourselves to isotropic hyperelastic behaviour in order to exclusively concentrate on the effects related to the orthotropic yield function derived in the next section. Moreover, elastic anisotropies in metals are expected to have a minor influence, therefore we might assume a volumetric deviatoric decoupled Neo-Hooke type material advocated by Simo (1988) which is formulated in terms of the isochoric elastic right Cauchy–Green tensor $\hat{\mathbf{C}}_e^{\flat} = J^{-2/3}\mathbf{C}_e^{\flat}$ and the elastic Jacobi determinant $J_e = \det \mathbf{F}_e$

$$\Psi^{mac} = \tfrac{1}{2}\mu[\hat{\mathbf{C}}_e^{\flat} : \mathbf{G}^{\#} - 3] + U(J_e) \quad \text{with} \quad U(J_e) = \kappa[J_e \ln J_e - J_e + 1]. \tag{10}$$

Here κ and μ correspond to the bulk modulus and shear modulus of the linear theory and $\mathbf{G}^{\#}$ denotes the contravariant metric in the plastic intermediate configuration. Then the second Piola–Kirchhoff stress tensor $\boldsymbol{\Sigma}_p^{\#}$ in $\mathscr{B}_p$ is computed as

$$\boldsymbol{\Sigma}_p^{\#} = \mu[\hat{\mathbf{G}}^{\#} - \tfrac{1}{3}[\hat{\mathbf{C}}_e^{\flat} : \mathbf{G}^{\#}]\mathbf{C}_e^{-1}] + JU'\mathbf{C}_e^{-1}. \tag{11}$$

Equivalently, the covariant representation $\mathbf{S}^{\flat}$ of the co-contravariant Mandel stress $\mathbf{S}$ follows in a volumetric deviatoric decoupled format with $\mathbf{G}^{\flat}$ the covariant metric in $\mathscr{B}_p$

$$\mathbf{S}^{\flat} = \mu[\hat{\mathbf{C}}_e^{\flat} - \tfrac{1}{3}[\hat{\mathbf{C}}_e^{\flat} : \mathbf{G}^{\#}]\mathbf{G}^{\flat}] + JU'\mathbf{G}^{\flat} = \mu\,\mathrm{dev}\,(\hat{\mathbf{C}}_e^{\flat}) + JU'\mathbf{G}^{\flat}. \tag{12}$$

For the micro part of the Helmholtz free energy Ψ^{mic} we assume the following function

$$\Psi^{mic} = [Y_\infty - Y_0]\left[q + \frac{\exp(-\kappa q) - 1}{\kappa}\right] + \tfrac{1}{2}Pq^2 \tag{13}$$

resulting in a saturation type law for the isotropic hardening

$$p(q) = [Y_\infty - Y_0][1 - \exp(-\kappa q)] + Pq. \tag{14}$$

Here Y_0 and Y_∞ denote the initial yield strength and the saturation strength, κ and P are an exponential and a linear hardening modulus.

4. ORTHOTROPIC YIELD FUNCTION

The aim of this section is the derivation of an orthotropic yield condition in terms of a symmetric second order anisotropy tensor in the plastic intermediate configuration. In the small strain regime Steinmann *et al.* (1994) demonstrated that the resulting formulation is related to the well-known Hill criterion (1948). In the sequel we will specify the intermediate configuration $\mathscr{B}_p$ to be isoclinic so that the axes of orthotropy in the reference configuration $\mathscr{B}_0$ and in the intermediate configuration are parallel. Thereby, a strong motivation is provided by the formulation of crystal plasticity in terms of slip planes and slip directions fixed in the intermediate configuration, see e.g. Asaro (1983). Along the same lines Lubarda (1994) describes anisotropic elastoplastic damage by second order damage variables which are elastically convected to the spatial configuration. In analogy the orthotropy axes are here considered to be convected with the material only during elastic deformation, i.e. if we describe orthotropy by three contra-covariant structural tensors $\mathbf{N}_I \otimes \mathbf{N}^I$ [see Boehler (1987)], their spatial counterparts are given by elastic push-forward

$$\mathbf{F}_e \cdot [\mathbf{N}_I \otimes \mathbf{N}^I] \cdot \mathbf{F}_e^{-1} = \mathbf{n}_i \otimes \mathbf{n}^i \quad \text{with} \quad i = I \quad \text{and} \quad \mathbf{N}_I \cdot \mathbf{N}^J = \delta_I^J \tag{15}$$

Then we sample the three structural tensors weighted by coefficients a_I into a symmetric second order contra-covariant anisotropy tensor $\mathbf{A}$

$$\mathbf{A} = \sum_{I=1}^{3} a_I \mathbf{N}_I \otimes \mathbf{N}^I \rightharpoonup \mathbf{a} = \mathbf{F}_e \cdot \mathbf{A} \cdot \mathbf{F}_e^{-1} = \sum_{I=1}^{3} a_I \mathbf{n}_i \otimes \mathbf{n}^i \tag{16}$$

Here we understand that the notion of symmetry only makes sense in connection with a metric, for example we have

$$\mathbf{A} \cdot \mathbf{G}^\# = [\mathbf{A} \cdot \mathbf{G}^\#]^t \qquad \text{or} \quad \mathbf{G}^\flat \cdot \mathbf{A} = [\mathbf{G}^\flat \cdot \mathbf{A}]^t$$

with

$$\mathbf{G}^\# = G^{IJ} \mathbf{G}_I \otimes \mathbf{G}_J \quad \text{or} \qquad \mathbf{G}^\flat = G_{IJ} \mathbf{G}^I \otimes \mathbf{G}^J. \tag{17}$$

An anisotropic scalar valued tensor function $\Phi(\mathbf{S})$, e.g. the yield condition, possesses symmetries in its argument $\mathbf{S}$ characterized by a symmetry group, here denoted by the subset RO(3) of the orthogonal group SO(3), such that the function $\Phi(\mathbf{S})$ is submitted to the following invariance condition

$$\Phi(\mathbf{S}) = \Phi(\mathbf{R} \cdot \mathbf{S} \cdot \mathbf{R}^t) \; \forall \, \mathbf{R} \in \mathrm{RO}(3). \tag{18}$$

It is common to call Φ a RO(3) invariant function of $\mathbf{S}$ [for a comprehensive introduction into the mathematical theory of representations for anisotropic tensor functions refer to Boehler (1987)]. Nevertheless, an anisotropic scalar valued tensor function $\Phi(\mathbf{S})$ in terms of the co-contravariant Mandel stress $\mathbf{S}$ is most conveniently represented as an isotropic scalar valued tensor function $\Phi(\mathbf{A}, \mathbf{S})$ in terms of the co-contravariant Mandel stress $\mathbf{S}$ and the contra-covariant anisotropy tensor $\mathbf{A}$ by the following irreducible integrity basis [see Boehler (1987)]

$$I_1^{\mathrm{str}} = \underline{[\mathbf{G}^\# \cdot \mathbf{S}] : \mathbf{G}^\flat}, \tag{19}$$

$$I_2^{\mathrm{str}} = [\mathbf{G}^\# \cdot \mathbf{S}] : [\mathbf{S} \cdot \mathbf{G}^\flat], \tag{20}$$

$$I_3^{\mathrm{str}} = [\mathbf{G}^\# \cdot \mathbf{S}^2] : [\mathbf{S} \cdot \mathbf{G}^\flat], \tag{21}$$

$$I_1^{\mathrm{ani}} = [\mathbf{A} \cdot \mathbf{G}^\#] : \mathbf{G}^\flat, \tag{22}$$

$$I_2^{\mathrm{ani}} = \underline{[\mathbf{A} \cdot \mathbf{G}^\#] : [\mathbf{G}^\flat \cdot \mathbf{A}]}, \tag{23}$$

$$I_3^{\mathrm{ani}} = [\mathbf{A}^2 \cdot \mathbf{G}^\#] : [\mathbf{G}^\flat \cdot \mathbf{A}], \tag{24}$$

$$I_1^{\mathrm{mix}} = [\mathbf{A}^\# \cdot \mathbf{S}] : \mathbf{G}^\flat, \tag{25}$$

$$I_2^{\mathrm{mix}} = [\mathbf{A}^\# \cdot \mathbf{S}] : \mathbf{S}^\flat, \tag{26}$$

$$I_3^{\mathrm{mix}} = \underline{[\mathbf{A}^\# \cdot \mathbf{S}] : \mathbf{A}^\flat}, \tag{27}$$

$$I_4^{\mathrm{mix}} = \underline{[\mathbf{A}^{\sharp}\cdot\mathbf{S}]:[\mathbf{S}\cdot\mathbf{A}^{\flat}]}. \tag{28}$$

Equivalently, we may express the integrity basis in terms of spatial anisotropy tensor $\mathbf{a}$ and the co-contravariant representation of the Kirchhoff stress $\boldsymbol{\tau} = \mathbf{F}_e^{-t}\cdot\mathbf{S}\cdot\mathbf{F}_e^{t}$ as

$$I_1^{\mathrm{str}} = \underline{[\mathbf{g}^{\sharp}\cdot\boldsymbol{\tau}]:\mathbf{g}^{\flat}}, \tag{29}$$

$$I_2^{\mathrm{str}} = [\mathbf{g}^{\sharp}\cdot\boldsymbol{\tau}]:[\boldsymbol{\tau}\cdot\mathbf{g}^{\flat}], \tag{30}$$

$$I_3^{\mathrm{str}} = [\mathbf{g}^{\sharp}\cdot\boldsymbol{\tau}^2]:[\boldsymbol{\tau}\cdot\mathbf{g}^{\flat}], \tag{31}$$

$$I_1^{\mathrm{ani}} = [\mathbf{a}\cdot\mathbf{g}^{\sharp}]:\mathbf{g}^{\flat}, \tag{32}$$

$$I_2^{\mathrm{ani}} = \underline{[\mathbf{a}\cdot\mathbf{g}^{\sharp}]:[\mathbf{g}^{\flat}\cdot\mathbf{a}]}, \tag{33}$$

$$I_3^{\mathrm{ani}} = [\mathbf{a}^2\cdot\mathbf{g}^{\sharp}]:[\mathbf{g}^{\flat}\cdot\mathbf{a}], \tag{34}$$

$$I_1^{\mathrm{mix}} = [\mathbf{a}^{\sharp}\cdot\boldsymbol{\tau}]:\mathbf{g}^{\flat}, \tag{35}$$

$$I_2^{\mathrm{mix}} = [\mathbf{a}^{\sharp}\cdot\boldsymbol{\tau}]:\boldsymbol{\tau}^{\flat}, \tag{36}$$

$$I_3^{\mathrm{mix}} = \underline{[\mathbf{a}^{\sharp}\cdot\boldsymbol{\tau}]:\mathbf{a}^{\flat}}, \tag{37}$$

$$I_4^{\mathrm{mix}} = \underline{[\mathbf{a}^{\sharp}\cdot\boldsymbol{\tau}]:[\boldsymbol{\tau}\cdot\mathbf{a}^{\flat}]}. \tag{38}$$

Based on the underlined invariants we propose the following orthotropic yield condition

$$\Phi(\mathbf{A},\mathbf{S}) = \Phi(\mathbf{a},\boldsymbol{\tau}) = \tfrac{1}{2}I_4^{\mathrm{mix}} - \tfrac{1}{3}I_1^{\mathrm{str}}I_3^{\mathrm{mix}} + \tfrac{1}{18}I_2^{\mathrm{ani}}[I_1^{\mathrm{str}}]^2 - \tfrac{1}{3}Y^2. \tag{39}$$

Note that this yield condition degenerates into the classical isotropic von Mises condition by identifying the anisotropy tensor $\mathbf{A} = \mathbf{G}^{\sharp}\cdot\mathbf{G}^{\flat}$ or $\mathbf{a} = \mathbf{g}^{\sharp}\cdot\mathbf{g}^{\flat}$ with the identity

$$\Phi(\mathbf{S}) = \Phi(\boldsymbol{\tau}) = \tfrac{1}{2}I_2^{\mathrm{str}} - \tfrac{1}{6}[I_1^{\mathrm{str}}]^2 - \tfrac{1}{3}Y^2 = \tfrac{1}{2}|\mathrm{dev}\,\mathbf{S}| - \tfrac{1}{3}Y^2 = \tfrac{1}{2}|\mathrm{dev}\,\boldsymbol{\tau}| - \tfrac{1}{3}Y^2. \tag{40}$$

To motivate this choice we proceed as follows: first, we restrict ourselves to a quadratic dependence of Φ on $\mathbf{S}$ with $\mathscr{A}$ a general fourth order tensor mapping symmetric second order tensors in the sense described above onto symmetric second order tensors, i.e.

$$\Phi = \Phi(\mathbf{S}:\mathscr{A}:\mathbf{S}) \doteq \Phi([\mathbf{R}\cdot\mathbf{S}\cdot\mathbf{R}^{t}]:\mathscr{A}:[\mathbf{R}\cdot\mathbf{S}\cdot\mathbf{R}^{t}]). \tag{41}$$

This expression is made more specific by introducing a certain structure for the fourth order anisotropy tensor $\mathscr{A}$ such that

$$\mathscr{A}:\mathbf{S} = \mathbf{A}^{\sharp}\cdot\mathbf{S}\cdot\mathbf{A}^{\flat} \rightsquigarrow \mathscr{A} = \tfrac{1}{2}[A^{IK}A_{LJ} + A^{I}_{\cdot L}A^{K}_{\cdot J}]\mathbf{G}_I\otimes\mathbf{G}^J\otimes\mathbf{G}_K\otimes\mathbf{G}^L. \tag{42}$$

Then, the invariance requirement in Eq. (18) leads to the representation

$$\Phi = \Phi(\mathbf{S}:[\mathbf{A}^{\#}\cdot\mathbf{S}\cdot\mathbf{A}^{\flat}]) \doteq \Phi(\mathbf{S}:[\mathbf{R}^{t}\cdot\mathbf{A}^{\#}\cdot\mathbf{R}\cdot\mathbf{S}\cdot\mathbf{R}^{t}\cdot\mathbf{A}^{\flat}\cdot\mathbf{R}]). \tag{43}$$

Thus, the choice of the second order anisotropy tensor $\mathbf{A}$ reduces to the set

$$\{\mathbf{A}|\mathbf{A} = \mathbf{R}^{t}\cdot\mathbf{A}\cdot\mathbf{R}, \forall\,\mathbf{R}\in \mathrm{RO}(3)\}. \tag{44}$$

For the isotropic case the reduced orthogonal group RO(3) of material symmetries coincides with the proper orthogonal group SO(3). Equivalently, for the transversly isotropic case with the plane of isotropy orthogonal e.g. to the $\mathbf{N}^3$ axis we have the reduced orthogonal group

$$\mathrm{RO}(3) \overset{\text{tra}}{=} \{\mathrm{SO}(2), \exp(\mathrm{spn}(\pi\mathbf{N}^1)), \exp(\mathrm{spn}(\pi\mathbf{N}^2))\}, \tag{45}$$

where we introduced the plane orthogonal group

$$\mathrm{SO}(2) = \{\mathbf{R}|\mathbf{R} = \exp(\mathrm{spn}(\alpha\mathbf{N}^3)), \quad \alpha\in[0,2\pi]\}. \tag{46}$$

Here, spn (•) and exp (spn (•)) denote the skew symmetric tensor and the rotation tensor associated with the axial vector (•), respectively. Finally, for orthotropy with the axes of orthotropy identical to the $\mathbf{N}^{\mathrm{I}}$ coordinate system the symmetries in $\mathbf{S}$ of Φ are described by the reduced orthogonal group

$$\mathrm{RO}(3) \overset{\text{ort}}{=} \{\exp(\mathrm{spn}(\pi\mathbf{N}^1)), \quad \exp(\mathrm{spn}(\pi\mathbf{N}^2)), \quad \exp(\mathrm{spn}(\pi\mathbf{N}^3))\}. \tag{47}$$

Clearly, for the cases of isotropy, transverse isotropy and orthotropy, respectively, it follows naturally that

$$A^{\mathrm{I}}_{\cdot\mathrm{J}} \overset{\text{iso}}{=} \begin{bmatrix} a & 0 & 0 \\ 0 & a & 0 \\ 0 & 0 & a \end{bmatrix}, \quad A^{\mathrm{I}}_{\cdot\mathrm{J}} \overset{\text{tra}}{=} \begin{bmatrix} a & 0 & 0 \\ 0 & a & 0 \\ 0 & 0 & a_3 \end{bmatrix}, \quad A^{\mathrm{I}}_{\cdot\mathrm{J}} \overset{\text{ort}}{=} \begin{bmatrix} a_1 & 0 & 0 \\ 0 & a_2 & 0 \\ 0 & 0 & a_3 \end{bmatrix}. \tag{48}$$

To construct an orthotropic yield criterion for metal elastoplasticity we introduce the fourth order mixed variant deviatoric projection operator

$$\mathscr{I}^{\mathrm{dev}} = \mathscr{I} - \tfrac{1}{3}[\mathbf{G}^{\flat}\cdot\mathbf{G}^{\#}]\otimes[\mathbf{G}^{\#}\cdot\mathbf{G}^{\flat}] \quad \text{with} \quad \mathscr{I} = \tfrac{1}{2}[\delta^{\cdot\mathrm{K}}_{\mathrm{I}\cdot}\delta^{\cdot\mathrm{J}}_{\mathrm{L}\cdot} + G_{\mathrm{IL}}G^{\mathrm{KJ}}]\mathbf{G}^{\mathrm{I}}\otimes\mathbf{G}_{\mathrm{J}}\otimes\mathbf{G}_{\mathrm{K}}\otimes\mathbf{G}^{\mathrm{L}}. \tag{49}$$

Then it is postulated that the yield condition depends exclusively on the deviatoric stresses

$$\Phi(\mathbf{A},\mathbf{S}) = \Phi(\mathbf{a},\boldsymbol{\tau}) = \Phi(\mathbf{S}:\mathscr{I}^{\mathrm{dev}}:\mathscr{A}:\mathscr{I}^{\mathrm{dev}}:\mathbf{S}) = \Phi(\mathbf{S}:\mathscr{P}:\mathbf{S}) \tag{50}$$

with the fourth order deviatoric anisotropy tensor

$$\mathscr{P} = \mathscr{A} - \tfrac{1}{3}[[\mathbf{G}^{\#}\cdot\mathbf{G}^{\flat}]\otimes\mathbf{A}^2 + \mathbf{A}^2\otimes[\mathbf{G}^{\#}\cdot\mathbf{G}^{\flat}]] + \tfrac{1}{9}I_2^{\mathrm{ani}}[\mathbf{G}^{\#}\cdot\mathbf{G}^{\flat}]\otimes[\mathbf{G}^{\#}\cdot\mathbf{G}^{\flat}]. \tag{51}$$

Next, equating $\mathbf{S}:\mathscr{P}:\mathbf{S}$ to a uniaxial reference yield stress Y gives exactly the yield condition proposed above and allows for an experimental determination of the three constants in $\mathbf{A}$, see Appendix B

$$\Phi(\mathbf{A},\mathbf{S}) = \Phi(\mathbf{a},\tau) = \tfrac{1}{2}\mathbf{S}:\mathscr{P}:\mathbf{S} - \tfrac{1}{3}Y^2 = 0. \tag{52}$$

Then the associated flow rule for the plastic velocity gradient on $\mathscr{B}_p$ follows straightforwardly,

$$\mathbf{L}_p = \gamma\,\partial_S\Phi = \gamma\mathscr{P}:\mathbf{S} = \gamma[\mathbf{A}^\sharp\cdot\mathbf{S}\cdot\mathbf{A}^\flat + \tfrac{1}{3}[\tfrac{1}{3}I_2^{ani}I_1^{str} - I_3^{mix}]\mathbf{G}^\sharp\cdot\mathbf{G}^\flat - \tfrac{1}{3}I_1^{str}\mathbf{A}^2] \tag{53}$$

Equivalently we obtain the spatial plastic velocity gradient $\mathbf{l}_p$ by push-forward

$$\mathbf{l}_p = \mathbf{F}_e\cdot\mathbf{L}_p\cdot\mathbf{F}_e^{-1} = \gamma[\mathbf{a}^\sharp\cdot\boldsymbol{\tau}\cdot\mathbf{a}^\flat + \tfrac{1}{3}[\tfrac{1}{3}I_2^{ani}I_1^{str} - I_3^{mix}]\mathbf{g}^\sharp\cdot\mathbf{g}^\flat - \tfrac{1}{3}I_1^{str}\mathbf{a}^2]. \tag{54}$$

For a linear dependence of Y on p, say $Y = Y_0 + p$, the associated evolution law for the hardening variable q is given by

$$\dot{q} = -\gamma\,\partial_p\Phi = \gamma\tfrac{2}{3}Y. \tag{55}$$

5. INTEGRATION ALGORITHM

This section is devoted to the algorithmic treatment of the orthotropic Hill type model within large strain multiplicative elastoplasticity discussed above. For small strain additive elastoplasticity an implicit integration algorithm for the Hill criterion was presented by de Borst and Feenstra (1990).

For the algorithmic integration we represent all tensors with respect to a fixed cartesian background coordinate system with base vectors $\mathbf{E}_I = \mathbf{E}^I$, i.e. the distinction between covariant and contravariant bases may be omitted. Within an incremental time stepping procedure the solution for the plastic deformation gradient is advanced from time step ${}^nt$ to time step ${}^{n+1}t$ via

$${}^{n+1}\mathbf{F}_p = \exp(\boldsymbol{\Lambda})\cdot{}^n\mathbf{F}_p \rightsquigarrow {}^{n+1}\mathbf{F}_e = {}^e\mathbf{F}_e\cdot\exp(-\boldsymbol{\Lambda}) \quad \text{with} \quad \boldsymbol{\Lambda} = \Delta\gamma\mathscr{P}:\operatorname{dev}\mathbf{S}. \tag{56}$$

Here, we introduced the algorithmic flow direction $\boldsymbol{\Lambda}$ which is symmetric due to the restriction to an isotropic hyperelastic constitutive law. The tensor exponential of the algorithmic flow direction defines a map from the set of deviatoric tensors onto the group of isochoric tensors $\exp(\bullet):\mathrm{sl}(3)\to\mathrm{SL}(3)$ and has the important property of conserving the plastic volume

$${}^{n+1}J_p = {}^nJ_p = 1 \quad \text{and} \quad {}^{n+1}J_e = {}^eJ_e. \tag{57}$$

The tensor exponential has recently been extensively applied within isotropic multiplicative elastoplasticity based on the spectral representation of symmetric tensors, e.g. Simo (1992), Miehe and Stein (1992), Steinmann *et al.* (1993) among many others. An exponential map algorithm for the treatment for anisotropic multiplicative elastoplasticity has been proposed by Miehe (1995).

To ease notation we omit the explicit indication of time step ${}^{n+1}t$ if there is no danger of confusion. With these preliminaries at hand the elastic right Cauchy-Green deformation tensor $\mathbf{C}_e$ follows straightforwardly in terms of the incremental plastic deformation gradient $\exp(\boldsymbol{\Lambda})$ and the trial elastic right Cauchy-Green tensor ${}^e\mathbf{C}_e = {}^e\mathbf{F}_e^t\cdot{}^e\mathbf{F}_e$ as

$$\mathbf{C}_e = \mathbf{F}_p^{-t}\cdot\mathbf{C}\cdot\mathbf{F}_p^{-1} = \exp(-\boldsymbol{\Lambda})\cdot{}^e\mathbf{C}_e\cdot\exp(-\boldsymbol{\Lambda}). \tag{58}$$

Additionally, the remaining evolution equation for the hardening variable is integrated fully implicitly to obtain

$$q = {}^{n}q + \Delta\gamma \tfrac{2}{3} Y. \tag{59}$$

The update formula for the deviatoric part of the Mandel stress $\mathbf{S}$ is then given by

$$\operatorname{dev}\mathbf{S} = \mu^* \mathscr{I}^{\operatorname{dev}} : [\exp(-\boldsymbol{\Lambda}) \cdot {}^{e}\mathbf{C}_e \cdot \exp(-\boldsymbol{\Lambda})] \quad \text{with} \quad \mu^* = \mu^e J_e^{-2/3}. \tag{60}$$

In the case of plastic loading we solve the nonlinear system of equations $\mathbf{R} = \mathbf{o}$ and the non-linear consistency condition $\Phi = 0$ with unknowns $\operatorname{dev}\mathbf{S}$ and $\Delta\gamma$ in a simultaneous iteration

$$\mathbf{R} = \operatorname{dev}\mathbf{S} - \mu^* \mathscr{I}^{\operatorname{dev}} : [\exp(-\boldsymbol{\Lambda}) \cdot {}^{e}\mathbf{C}_e \cdot \exp(-\boldsymbol{\Lambda})] \tag{61}$$

$$\Phi = \tfrac{1}{2} \operatorname{dev}\mathbf{S} : \mathscr{P} : \mathbf{S} - \tfrac{1}{3} Y^2. \tag{62}$$

To establish an iteration operator within a Newton type scheme we make use of the following approximation to the variation of $\exp(\boldsymbol{\Lambda})$ which is exact as long as the eigen-directions of $\boldsymbol{\Lambda}$ do not change

$$\delta \exp(\boldsymbol{\Lambda}) \approx \exp(\boldsymbol{\Lambda}) \cdot \delta\boldsymbol{\Lambda}. \tag{63}$$

Numerical experience prove that this condition is uncritical in the sense that the iteration converges quasi quadratic even in the case of simple shear. The simple structure of this approximation, on the other hand, makes it easy to come up with an iteration operator for the nonlinear equation system above. The ingredients of the iteration operator are then computed with the abbreviation $\mathbf{s} = \operatorname{dev}\mathbf{S}$

$$\partial_{\mathbf{s}}\mathbf{R} = \mathscr{I} + \Delta\gamma\mu^* \mathscr{I}^{\operatorname{dev}} : [\mathscr{P} \cdot \mathbf{C}_e + \mathbf{C}_e \cdot \mathscr{P}] \tag{64}$$

$$\gamma_\gamma \mathbf{R} = \mu^* \mathscr{I}^{\operatorname{dev}} : [\mathbf{s} : \mathscr{P} \cdot \mathbf{C}_e + \mathbf{C}_e \cdot \mathscr{P} : \mathbf{s}] \tag{65}$$

$$\partial_{\mathbf{s}}\Phi = \mathscr{P} : \mathbf{s} \tag{66}$$

$$\partial_\gamma \Phi = \frac{4Y^2 p'}{6\Delta\gamma p' - 9}. \tag{67}$$

With these preliminaries at hand we obtain the iterative correction for the plastic multiplier

$$\Delta\Delta\gamma = \frac{\Phi - \partial_{\mathbf{s}}\Phi : [\partial_{\mathbf{s}}\mathbf{R}]^{-1} : \mathbf{R}}{\partial_{\mathbf{s}}\Phi : [\partial_{\mathbf{s}}\mathbf{R}]^{-1} : \partial_\gamma \mathbf{R} - \partial_\gamma \Phi} \tag{68}$$

and the solutions for $\Delta\gamma$ and $\mathbf{s}$ are updated successively

$$\Delta\gamma = \Delta\gamma + \Delta\Delta\gamma \quad \text{and} \quad \mathbf{s} = \mathbf{s} - [\partial_{\mathbf{s}}\mathbf{R}]^{-1} : [\mathbf{R} + \Delta\Delta\gamma\, \partial_\gamma \mathbf{R}]. \tag{69}$$

The iteration stops as soon as both the residuum and the nonlinear consistency condition satisfy

$$|\mathbf{R}| \leqslant 10^{-10} \quad \text{and} \quad \Phi \leqslant 10^{-10}. \tag{70}$$

The domain of convergence of the overall iteration is considerably enlarged by including some separate iterations for the residuum $\mathbf{R}$ at fixed $\Delta\gamma$ with

$$\mathbf{s} = \mathbf{s} - [\partial_{\mathbf{s}}\mathbf{R}]^{-1} : \mathbf{R} \quad \text{until} \quad |\mathbf{R}| \leqslant 10^{-1}. \tag{71}$$

The iteration operator is given in a matrix format in the Appendix.

6. ENHANCED PLANE STRESS ELEMENT FORMULATION

Next we are concerned with the dynamic extension of a plane finite element formulation which satisfies the plane stress constraint in a weak sense, see Steinmann *et al.* (1995), allowing for the incorporation of arbitrary large strain 3D constitutive models. The key issue is to equip the element with a thickness field as a primary variable thus allowing for thickness changes. To this end we introduce the following decomposition of the reference and the spatial configuration into a plane midsurface domain $\bar{\mathcal{B}}_0$ and the thickness $\mathcal{H}_0$ as

$$\mathcal{B}_0 = \bar{\mathcal{B}}_0 \times \mathcal{H}_0 \quad \text{and} \quad \mathcal{B} = \bar{\mathcal{B}} \times \mathcal{H} \quad \text{with} \quad \bar{\mathcal{B}}_0 \subset \mathbb{R}^2 \quad \text{and} \quad \mathcal{H}_0 : \bar{\mathcal{B}}_0 \to [-H/2, H/2]. \tag{72}$$

Furthermore, we assume that all external loading acts exclusively in the midsurface plane and that all midsurface deformations are restricted to the midsurface domain. This excludes for example out of plane bending or buckling. As a consequence the nonlinear deformation map $\boldsymbol{\varphi}(\mathbf{X})$ splits into the midsurface deformation $\boldsymbol{\varphi}_{\mathrm{m}}(\bar{\mathbf{X}}) \in \mathbb{R}^3$ and the out of plane deformation $\boldsymbol{\varphi}_{\mathrm{t}}(\mathbf{X}) \in \mathbb{R}^3$ with representation in cartesian coordinates

$$\boldsymbol{\varphi}_{\mathrm{m}}(\bar{\mathbf{X}}) = \begin{bmatrix} \bar{\boldsymbol{\varphi}}(\bar{\mathbf{X}}) \\ 0 \end{bmatrix} \quad \text{and} \quad \boldsymbol{\varphi}_{\mathrm{t}}(\mathbf{X}) = \begin{bmatrix} \mathbf{o}_{(2\times 1)} \\ \varphi_3(\mathbf{X}) \end{bmatrix} \quad \text{with} \quad \begin{matrix} \bar{\mathbf{x}} = \bar{\boldsymbol{\varphi}}(\bar{\mathbf{X}}) \in \mathbb{R}^2 \\ x_3 = \varphi_3(\mathbf{X}) \in \mathbb{R} \end{matrix} \tag{73}$$

In addition to the 3D gradient operators $\nabla_{\mathrm{X}}(\bullet)$ and $\nabla_{\mathrm{x}}(\bullet)$ we define in plane gradient operators $\bar{\nabla}_{\mathrm{X}}(\bullet)$ and $\bar{\nabla}_{\mathrm{x}}(\bullet)$. With these preliminaries at hand the deformation gradient $\mathbf{F} : T\mathcal{B}_0 \to T\mathcal{B}$ separates into two parts with $\bar{\mathbf{F}} : T\bar{\mathcal{B}}_0 \to T\bar{\mathcal{B}}$ the in plane deformation gradient

$$\mathbf{F} = \nabla_{\mathrm{X}}\boldsymbol{\varphi} = \begin{bmatrix} \bar{\nabla}_{\mathrm{X}}\bar{\boldsymbol{\varphi}} & \mathbf{o}_{(2\times 1)} \\ \bar{\nabla}_{\mathrm{X}}\varphi_3 & \varphi_{3,\mathrm{X}_3} \end{bmatrix} = \begin{bmatrix} \bar{\mathbf{F}} & \mathbf{o}_{(2\times 1)} \\ \bar{\nabla}_{\mathrm{X}}\varphi_3 & \varphi_{3,\mathrm{X}_3} \end{bmatrix} \tag{74}$$

In the sequel we resort to the enhanced assumed element approach advocated in Simo and Rifai (1990) (geometrically linear) and Simo and Armero (1992) (geometrically nonlinear) for the improvement of the inplane bending behaviour. Within the geometrically nonlinear continuum theory the underlying idea of the enhanced formulation was originally presented in Simo and Armero (1992) and consists in the additive split of the displacement gradient $\mathbf{H}$ into a compatible and an enhanced contribution $\mathbf{H} = \nabla_{\mathrm{X}}\mathbf{u} + \tilde{\mathbf{H}}$. Due to the subsidary conditions $\tilde{\mathbf{H}} = \mathbf{o}$ independent assumed first Piola-Kirchhoff stresses $\boldsymbol{\Sigma}_{\mathrm{I}}$ enter the underlying mixed variational principle as Lagrange parameter. We will directly proceed to the enhanced discrete version of the weak form of balance of linear momentum in the 3D spatial setting with $\tilde{\nabla}_{\mathrm{x}}(\bullet) = \nabla_{\mathrm{X}}(\bullet) \cdot \mathbf{F}^{-1}$ and $\tilde{\mathbf{h}} = \tilde{\mathbf{H}} \cdot \mathbf{F}^{-1}$.

$$\int_{\mathcal{B}_0} [\rho_0 \delta\boldsymbol{\varphi}^{\mathrm{h}} \cdot \ddot{\boldsymbol{\varphi}}^{\mathrm{h}} + [\tilde{\nabla}_{\mathrm{x}}\delta\boldsymbol{\varphi}^{\mathrm{h}} + \delta\tilde{\mathbf{h}}^{\mathrm{h}}] : \boldsymbol{\tau}^{\mathrm{t}}] \, \mathrm{d}V = \int_{\mathcal{B}_0} \delta\boldsymbol{\varphi}^{\mathrm{h}} \cdot \mathbf{B}\rho_0 \, \mathrm{d}V + \int_{\partial\mathcal{B}_0^{\mathrm{t}}} \delta\boldsymbol{\varphi}^{\mathrm{h}} \cdot \mathbf{t}_0^{\mathrm{p}} \, \mathrm{d}A \tag{75}$$

Here the incorporated L_2-orthogonality of the discrete form of the assumed first Piola-Kirchhoff stress $\boldsymbol{\Sigma}_{\mathrm{I}}^{\mathrm{h}}$ and the enhanced displacement gradient $\tilde{\mathbf{H}}^{\mathrm{h}}$, originally proposed in Simo and Rifai (1990) for the geometrically linear case, eliminated the explicit appearance of the assumed stress field in the discretized variational formulation

$$\int_{\mathscr{B}_0} \delta\boldsymbol{\Sigma}_1^{h,t} : \tilde{\mathbf{H}}^h \, dV = 0. \tag{76}$$

Next we focus on the isoparametric discretization of the domain $\mathscr{B}_0 = \bigcup_{e=1}^{n_{el}} \mathscr{B}_{0e} \subset \mathbb{R}^3$. For a four-noded element with $n_{en} = 4$ the midsurface position $\bar{\mathbf{X}}^h : \square \to \bar{\mathscr{B}}_{0e}$ and the midsurface deformation map $\bar{\boldsymbol{\varphi}}^h : \square \to \bar{\mathscr{B}}_e$ together with its variation and acceleration are approximated by bilinear expansions $N^k(\bar{\boldsymbol{\xi}})$ with $\bar{\boldsymbol{\xi}}$ the coordinates of the plane isoparametric domain $\square$

$$\bar{\mathbf{X}}^h = \sum_{k=1}^{n_{en}} N^k \bar{\mathbf{X}}_k, \quad \bar{\boldsymbol{\varphi}}^h = \sum_{k=1}^{n_{en}} N^k \bar{\mathbf{x}}_k \quad \text{and} \quad \delta\bar{\boldsymbol{\varphi}}^h = \sum_{k=1}^{n_{en}} N^k \delta\bar{\mathbf{x}}_k, \quad \ddot{\bar{\boldsymbol{\varphi}}}^h = \sum_{k=1}^{n_{en}} N^k \ddot{\bar{\mathbf{x}}}_k. \tag{77}$$

Equivalently, we discretize the out of plane position $X_3^h : [-1, 1] \to \mathbb{R}$ and the out of plane deformation map $\varphi_3^h : [-1, 1] \to \mathbb{R}$ together with its variation and acceleration parametrized in the node point thickness as

$$X_3^h = \sum_{k=1}^{n_{en}} N_3^k H_k, \quad \varphi_3^h = \sum_{k=1}^{n_{en}} N_3^k h_k \quad \text{and} \quad \delta\varphi_3^h = \sum_{k=1}^{n_{en}} N_3^k \delta h_k, \quad \ddot{\varphi}_3^h = \sum_{k=1}^{n_{en}} N_3^k \ddot{h}_k. \tag{78}$$

Thereby, the shape functions $N_3^k(\boldsymbol{\xi})$ are defined as

$$N_3^k = \tfrac{1}{2}\xi_3 N^k(\bar{\boldsymbol{\xi}}) \rightsquigarrow \boldsymbol{\varphi}(\mathbf{X}) = \boldsymbol{\varphi}_m(\bar{\mathbf{X}}) + \tfrac{1}{2}\xi_3 h(\bar{\mathbf{X}})\mathbf{E}_3. \tag{79}$$

Here $H(\bar{\mathbf{X}})$ and $h(\bar{\mathbf{X}})$ denote the initial and the current thickness discretized by bilinear expansion

$$H^h = \sum_{k=1}^{n_{en}} N^k H_k, \quad h^h = \sum_{k=1}^{n_{en}} N^k h_k \quad \text{and} \quad \delta h^h = \sum_{k=1}^{n_{en}} N^k \delta h_k, \quad \ddot{h}^h = \sum_{k=1}^{n_{en}} N^k \ddot{h}_k. \tag{80}$$

Clearly, this concept is borrowed from shell theory with extensible director, e.g. Betsch *et al.* (1995) or Büchter *et al.* (1994) and references therein, where we have a natural kinematical split into the midsurface deformation and the director deformation. In our case the director with length $\frac{1}{2}h(\bar{\mathbf{X}})$ has a fixed orientation coaxial to the global $\mathbf{E}_3$ direction. The 3D Jacobi matrix of the reference placement and the in plane Jacobi matrix are denoted by $\mathbf{J} : T\square \to T\mathscr{B}_0$ with $j = \det \mathbf{J}$ and $\bar{\mathbf{J}} : T\square \to T\bar{\mathscr{B}}_0$ with $\bar{j} = \det \bar{\mathbf{J}}$. Here the dimension of the isoparametric domain $\square$ depends on the context. Moreover we introduce the constant Jacobi matrices $\mathbf{J}_0 = \mathbf{J}(\boldsymbol{\xi} = \mathbf{o})$ and $\bar{\mathbf{J}}_0 = \bar{\mathbf{J}}(\bar{\boldsymbol{\xi}} = \mathbf{o})$ with $j_0 = \det \mathbf{J}_0$ and $\bar{j}_0 = \det \bar{\mathbf{J}}_0$ at the centroid of the element.

The key assumptions for exact plane stress analysis are on the one hand vanishing out-of-plane normal Cauchy stresses $\sigma_{33} = 0$ and on the other hand the neglect of all transverse shear stresses and strains. As will be demonstrated later the first requirement is satisfied in a weak sense by the present approach while the latter is a direct consequence of restricting the numerical quadrature to the midsurface plane. Another advantage of the explicit restriction to an one layer integration is the reduction of the dimension of the discrete strain operators. Here the numerical costs are in the order of an axial symmetric computation. Then the inplane and out of plane contributions to the Jacobi matrix, the deformation gradient and the spatial velocity gradient decouple

$$\mathbf{J} = \begin{bmatrix} \bar{\mathbf{J}} & \mathbf{o}_{(2\times 1)} \\ \mathbf{o}_{(1\times 2)} & \frac{1}{2}H^h \end{bmatrix}, \quad \mathbf{F}^h = \begin{bmatrix} \bar{\mathbf{F}}^h & \mathbf{o}_{(2\times 1)} \\ \mathbf{o}_{(1\times 2)} & h^h/H^h \end{bmatrix} \quad \text{and} \quad \mathbf{l}^h = \begin{bmatrix} \bar{\mathbf{l}}^h & \mathbf{o}_{(2\times 1)} \\ \mathbf{o}_{(1\times 2)} & \delta h^h/h^h \end{bmatrix}. \tag{81}$$

For a suitable approximation of the enhanced displacement gradient field $\tilde{\mathbf{H}}^h$ we restrict ourselves to an inplane enhancement in the form

$$\tilde{\bar{\mathbf{H}}}^{h} = \sum_{k=1}^{2} \boldsymbol{\alpha}_k \otimes \tilde{\mathbf{e}}_0^k \quad \text{and} \quad \tilde{\bar{\mathbf{h}}}^{h} = \sum_{k=1}^{2} \boldsymbol{\alpha}_k \otimes \tilde{\mathbf{e}}^k \quad \text{with} \quad \tilde{\mathbf{e}}^k = \bar{\mathbf{F}}^{-t} \cdot \tilde{\mathbf{e}}_0^k. \tag{82}$$

Here $\boldsymbol{\alpha}_k \in \mathbb{R}^2$ are vectors of internal degrees of freedom and $\tilde{\mathbf{e}}_0^k \in \mathbb{R}^2$ denote linearly independent vectors of shape functions. Conditions and restrictions regarding the choice of the $\tilde{\mathbf{e}}_0^k$ were elaborated in Simo and Rifai (1990) and Simo and Armero (1992). Push-forward into the spatial representation is performed with the enhanced deformation gradient $\bar{\mathbf{F}} = \bar{\mathbf{I}} + \bar{\nabla}_X \bar{\mathbf{u}} + \tilde{\bar{\mathbf{H}}}$. It has to be emphasized that the actual choice for the first Piola-Kirchhoff stress approximation enters the iterative global equilibrium solution at no stage if the L_2-orthogonality condition between the assumed first Piola-Kirchhoff stress field and the enhanced displacement gradient is (elementwise) exactly satisfied by construction. For the vectors of shape functions we choose the following classical approximations with $j = \frac{1}{2}\bar{j}H$ and $j_0 = \frac{1}{2}\bar{j}_0 H_0$

$$\tilde{\mathbf{e}}_0^k = \frac{j_0}{j} \bar{\mathbf{J}}_0^{-t} \cdot \mathbf{e}_0^k \quad \text{with} \quad \mathbf{e}_0^1 = \begin{bmatrix} \xi_1 \\ 0 \end{bmatrix} \quad \text{and} \quad \mathbf{e}_0^2 = \begin{bmatrix} 0 \\ \xi_2 \end{bmatrix}. \tag{83}$$

Note that the vectors of shape functions $\mathbf{e}_0^k$ can be related to the classical incompatible midsurface deformation map proposed originally by Taylor *et al.* (1976)

$$\bar{\boldsymbol{\varphi}}_{inc}^{h} = \sum_{k=1}^{n_{en}} N^k \bar{\mathbf{x}}_k + \sum_{k=1}^{2} N_{inc}^k \boldsymbol{\alpha}_k \quad \text{with} \quad N_{inc}^k = \tfrac{1}{2}[\xi_k^2 - 1]. \tag{84}$$

Finally the enhanced discretized weak form of the balance of linear momentum decouples into the inplane plane contribution which writes for a constant initial thickness H^h

$$\int_{\bar{\mathcal{B}}_0} [\rho_0 \delta\bar{\boldsymbol{\varphi}}^h \cdot \ddot{\bar{\boldsymbol{\varphi}}}^h + [\tilde{\bar{\nabla}}_x \delta\bar{\boldsymbol{\varphi}}^h + \delta\tilde{\bar{\mathbf{h}}}^h] : \bar{\boldsymbol{\tau}}^t] \, \mathrm{d}\bar{V} = \int_{\bar{\mathcal{B}}_0} \delta\bar{\boldsymbol{\varphi}}^h \cdot \bar{\mathbf{B}} \rho_0 \, \mathrm{d}\bar{V} + \int_{\partial\bar{\mathcal{B}}_0^t} \delta\bar{\boldsymbol{\varphi}}^h \cdot \bar{\mathbf{t}}_0^R \, \mathrm{d}\bar{A} \tag{85}$$

and an out of plane contribution containing as a key message the plane stress condition $\sigma_{33} = 0$ which is indeed satisfied in a weak sense for vanishing current thickness $h^h \to 0$, i.e. in the discretized version this condition will be satisfied with mesh densification, see Steinmann *et al.* (1995)

$$\frac{1}{12} \int_{\bar{\mathcal{B}}} \delta h^h \ddot{h}^h \rho h^h \, \mathrm{d}\bar{V} + \int_{\bar{\mathcal{B}}} \delta h^h \sigma_{33} \, \mathrm{d}\bar{v} = 0. \tag{86}$$

Here the out of plane prescribed tractions and body forces have been set to zero in accordance with the assumption of a plane stress analysis. The matrix format of the equilibrium equations is written in an obvious manner with $\mathbf{d}_e \in \mathbb{R}^8$ and $\mathbf{h}_e \in \mathbb{R}^4$ the in plane and out of plane element nodal degrees of freedom and $\bar{\mathbf{m}}_e$ and $\mathbf{m}_e^3$ the associated mass matrices

$$\begin{aligned} \bigcup_{e=1}^{n_{el}} \; & \bar{\mathbf{m}}_e \cdot \ddot{\mathbf{d}}_e + \bar{\mathbf{f}}_e^{int} = \bigcup_{e=1}^{n_{el}} \bar{\mathbf{f}}_e^{ext} \\ \bigcup_{e=1}^{n_{el}} \; & \mathbf{m}_e^3 \cdot \ddot{\mathbf{h}}_e + \mathbf{f}_e^{int,3} = \mathbf{o} \\ \forall_{e=1}^{n_{el}} \; & \tilde{\bar{\mathbf{f}}}_e^{int} = \mathbf{o}. \end{aligned} \tag{87}$$

The enhanced four-noded element described above is designed to reproduce the plane stress state in the weak sense and is denoted by Q1TE4.

7. EXPLICIT SOLUTION STRATEGY

In order to obtain a truly explicit solution strategy the element internal degrees of freedom $\boldsymbol{\alpha}_e \in \mathbb{R}^4$ are equipped with independent inertia terms which are motivated by the concept of an incompatible midsurface deformation map. Thereby the incompatible shape functions N^k_{inc} serve as a basis for the associated mass matrix $\tilde{\mathbf{m}}_e$. Upon diagonalizing the mass matrices the following semidiscrete equations of motion have to be integrated in time

$$\begin{aligned}
&\bigcup_{e=1}^{n_{el}} \lceil \bar{\mathbf{m}}_e \rfloor \cdot \ddot{\mathbf{d}}_e + \bar{\mathbf{f}}_e^{int} = \bigcup_{e=1}^{n_{el}} \bar{\mathbf{f}}_e^{ext} \quad \rightsquigarrow \bar{\mathbf{M}} \cdot \ddot{\mathbf{d}} + \bar{\mathbf{F}}^{int}(\mathbf{d}, \mathbf{h}, \boldsymbol{\alpha}) = \bar{\mathbf{F}}^{ext} \\
&\bigcup_{e=1}^{n_{el}} \beta_e \lceil \mathbf{m}_e^3 \rfloor \cdot \ddot{\mathbf{h}}_e + \mathbf{f}_e^{int,3} = \mathbf{o} \quad \rightsquigarrow \mathbf{M}_3 \cdot \ddot{\mathbf{h}} + \mathbf{F}_3^{int}(\mathbf{d}, \mathbf{h}, \boldsymbol{\alpha}) = \mathbf{o} \\
&\forall_{e=1}^{n_{el}} \lceil \tilde{\mathbf{m}}_e \rfloor \cdot \ddot{\boldsymbol{\alpha}}_e + \tilde{\bar{\mathbf{f}}}_e^{int} = \mathbf{o} \quad \rightsquigarrow \tilde{\mathbf{M}} \cdot \ddot{\boldsymbol{\alpha}} + \tilde{\bar{\mathbf{F}}}^{int}(\mathbf{d}, \mathbf{h}, \boldsymbol{\alpha}) = \mathbf{o}
\end{aligned} \tag{88}$$

Here the $\lceil \bullet \rfloor$ denote the lumped mass matrices which are obtained by applying the row sum technique to the consistent mass matrices. Moreover, a linear eigenvalue analysis reveals that the lumped out of plane element mass matrix has to be scaled by a factor $\beta_e \propto \int_{\mathcal{B}_{0e}} H^{-2}\, d\bar{V}$ in order to achieve effective critical time steps in an explicit analysis, compare the arguments presented in Hughes (1987) and references therein in the context of rotational degrees of freedom. Thereby, the essential idea is to reduce the maximum eigenfrequency associated with out of plane vibrations to the order of inplane eigenfrequencies. Then the explicit time stepping algorithm for the semidiscrete equations of motion tailored for the enhanced plane stress element is outlined in the following box:

1. Solution for new accelerations at time ${}^n t$ from

$$\begin{aligned}
\bar{\mathbf{M}} \cdot {}^n\ddot{\mathbf{d}} &= {}^n\bar{\mathbf{F}}^{ext} - \bar{\mathbf{F}}^{int}({}^n\mathbf{d}, {}^n\mathbf{h}, {}^n\boldsymbol{\alpha}) \\
\mathbf{M}^3 \cdot {}^n\ddot{\mathbf{h}} &= \quad - \mathbf{F}_3^{int}({}^n\mathbf{d}, {}^n\mathbf{h}, {}^n\boldsymbol{\alpha}) \\
\tilde{\mathbf{M}} \cdot {}^n\ddot{\boldsymbol{\alpha}} &= \quad - \tilde{\bar{\mathbf{F}}}^{int}({}^n\mathbf{d}, {}^n\mathbf{h}, {}^n\boldsymbol{\alpha})
\end{aligned}$$

2. Update of predictor values

$$\begin{aligned}
{}^{n+1}\mathbf{d} &= {}^n\mathbf{d} + \Delta t\, {}^n\dot{\mathbf{d}}_p + \Delta t^2\, {}^n\ddot{\mathbf{d}} \quad \text{and} \quad {}^{n+1}\dot{\mathbf{d}}_p = {}^n\dot{\mathbf{d}}_p + \Delta t\, {}^n\ddot{\mathbf{d}} \\
{}^{n+1}\mathbf{h} &= {}^n\mathbf{h} + \Delta t\, {}^n\dot{\mathbf{h}}_p + \Delta t^2\, {}^n\ddot{\mathbf{h}} \quad \text{and} \quad {}^{n+1}\dot{\mathbf{h}}_p = {}^n\dot{\mathbf{h}}_p + \Delta t\, {}^n\ddot{\mathbf{h}} \\
{}^{n+1}\boldsymbol{\alpha} &= {}^n\boldsymbol{\alpha} + \Delta t\, {}^n\dot{\boldsymbol{\alpha}}_p + \Delta t^2\, {}^n\ddot{\boldsymbol{\alpha}} \quad \text{and} \quad {}^{n+1}\dot{\boldsymbol{\alpha}}_p = {}^n\dot{\boldsymbol{\alpha}}_p + \Delta t\, {}^n\ddot{\boldsymbol{\alpha}}
\end{aligned}$$

3. Compute internal forces and in plane loading ${}^{n+1}\bar{\mathbf{F}}^{ext}$ at time ${}^{n+1}t$

$$\begin{aligned}
{}^{n+1}\bar{\mathbf{F}}^{int} &= \bar{\mathbf{F}}^{int}({}^{n+1}\mathbf{d}, {}^{n+1}\mathbf{h}, {}^{n+1}\boldsymbol{\alpha}) \\
{}^{n+1}\mathbf{F}_3^{int} &= \mathbf{F}_3^{int}({}^{n+1}\mathbf{d}, {}^{n+1}\mathbf{h}, {}^{n+1}\boldsymbol{\alpha}) \\
{}^{n+1}\tilde{\bar{\mathbf{F}}}^{int} &= \tilde{\bar{\mathbf{F}}}^{int}({}^{n+1}\mathbf{d}, {}^{n+1}\mathbf{h}, {}^{n+1}\boldsymbol{\alpha})
\end{aligned}$$

4. Set time step counter to $n = n+1$ and goto 1

Box 1. Explicit time stepping algorithm.

8. DYNAMIC PLANE STRESS EXTENSION OF A THIN SHEET

In this example we consider a homogeneous plane stress tension problem of an orthotropic elastoplastic specimen under dynamic loading conditions. Thereby, the motivation is provided by catastrophic loading cases or metal forming where high speed deformations of thin metal sheets are very likely to occur. Within this scenario we focus especially on the tremendous influence of the out of plane orthotropy on the resulting failure mode.

The geometry of the specimen with width of 6.413 mm, height of 26.667 mm and constant initial thickness $H = 0.1$ mm is discretized into 10×20 plane stress Q1TE4 finite elements. The boundary conditions prohibit the vertical movement of the bottom surface and are free everywhere else. The final vertical elongation of 5 mm is applied in 20 000 time steps with $\Delta t = 2.5 \times 10^{-8}$s by a constant prescribed velocity of $v = 10$ m s^{-1} subjected to the top surface. We employ the explicit time stepping algorithm outlined above.

For the material parameters we assume typical values frequently employed in numerical simulations of ductile metals. The elastic constants are $K = 164.21$ GPa and $\mu = 80.1938$ GPa, the density is assumed as $\rho = 8000$ kg m^{-3}, the initial yield strength is set to $Y_0 = 0.45$ GPa, isotropic hardening is modelled by the saturation type law with saturation strength $Y_\infty = 0.715$ GPa, exponent $\kappa = 16.93$ and linear softening modulus $P = -0.012924$ GPa. The small amount of softening in P was introduced to trigger localization and might be interpreted as the simplest phenomenological description of internal material deterioration, see Steinmann *et al.* (1993).

We investigate three different cases (a)–(c) of transverse isotropy with the plane of isotropy orthogonal to the global $\mathbf{E}^3$ direction, i.e. we vary the ratio between the yield strength in the global $\mathbf{E}^3$ direction and the yield strength in the computational plane

$$r = Y_{33}/Y_{11} = Y_{33}/Y_{22} = Y_{33}/Y \quad \text{with} \quad r_a = \sqrt{0.5}, \quad r_b = 1, \quad r_c = 2 \tag{89}$$

in the following finite element analysis. Depending on the degree of transverse isotropy, different failure modes emerge within this problem. This investigation is motivated by the analysis for the geometrically linear case in Steinmann *et al.* (1994) which examined the influence of the out of plane orthotropy on the in plane orientation of possible localization zones.

Recall that localization denotes the onset of a discontinous bifurcation in the form of a jump in the spatial velocity gradient field, see e.g. Mandel (1966) or Rice (1976). At the constitutive level the formation of a spatial discontinuity across a singularity surface is signalled by the localization condition which manifests itself in the form of a singularity of the localization tensor which may be conceived as the projection of the tangential material operator onto a singularity surface. It has to be emphasized that the spatial orientation of the discontinuity is determined by the underlying constitutive model and the stress state. For a comparison we refer to the early plane strain localization computations which have been pioneered by Tvergaard *et al.* (1981) and are summarized in the overview article by Needleman and Tvergaard (1984).

Within the geometrically linear localization analysis at the constitutive level in Steinmann *et al.* (1994) a uniaxial plane stress state results in a discontinuity normal oriented with 0° with respect to the axis of tension for case (a), an orientation of 35.26° for the isotropic case (b) and finally a discontinuity at 43.09° for case (c). The aim of the present study is to oppose those findings with the results of a geometrically nonlinear numerical analysis under dynamical loading conditions. The qualification of enhanced element formulations to capture localized failure modes was pointed out in Steinmann and Willam (1991). Thereby, the formation of a localized zone is triggered by a small pertubation introduced by reducing the yield strength and the saturation strength to 90% at the outer left and right bottom elements for the case (a) and at the left bottom element for the cases (b) and (c). Observe that we introduced a small amount of softening.

Different failure modes participate within this problem. In the first part of the load history the boundary conditions allow the specimen to remain in an essentially homogeneous deformation pattern. In an advanced state of loading this diffuse mode of elongation gives way to localized failure patterns with large accumulated inelastic strains leading to the final failure of the specimen in reality. The results of the analysis are displayed in Figs 1–3 for the cases (a)–(c). We monitored the development of the deformed configurations, the distribution of the plastic zone in terms of the internal variable q and the thickness stretch at time steps 15 000, 17 500 and 20 000.

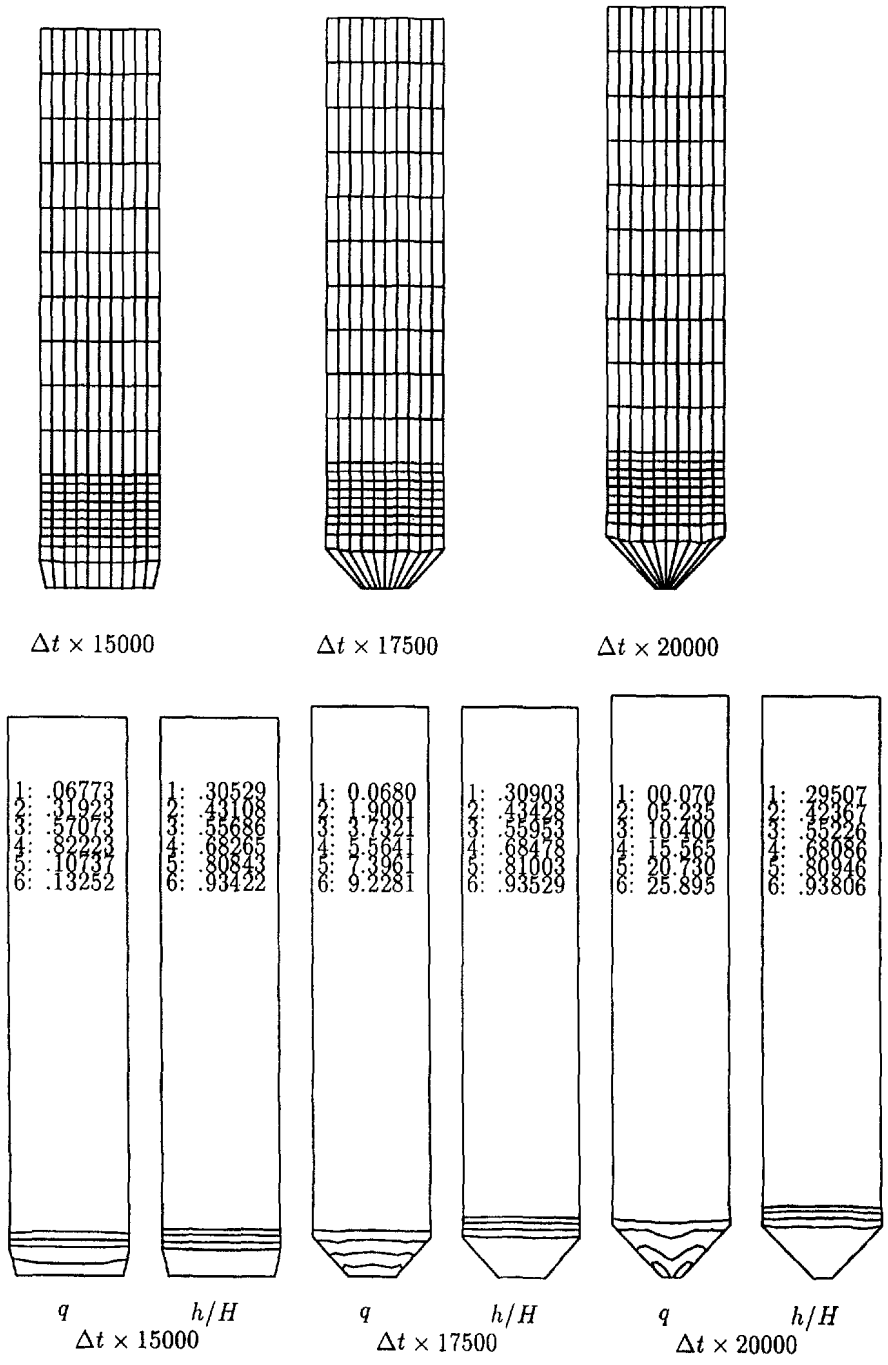

Fig. 1. Dynamic plane stress extension of a thin sheet: case (a).

The distribution of the plastic zone and the thickness stretch h/H reflect the tendency to develop different failure modes. The choice (a) leads to a brittle splitting tension mode, choice (c) renders almost a ductile shear band failure mode while the isotropic case (b) results in a mixed failure mode. Thereby, the orientation of the failure bands of the geometrically nonlinear numerical analysis under dynamical loading conditions is in close agreement with that predicted within the quasistatic geometrically linear setting. The intriguing influence of the out of plane orthotropy on the orientation of the in plane failure bands is neatly retrofitted. Clearly, after the onset of localization the stress state ceases to be homogeneous, thus blurring the picture given by the analytical prediction under perfect homogeneous conditions. This becomes especially apparent for the isotropic case where a

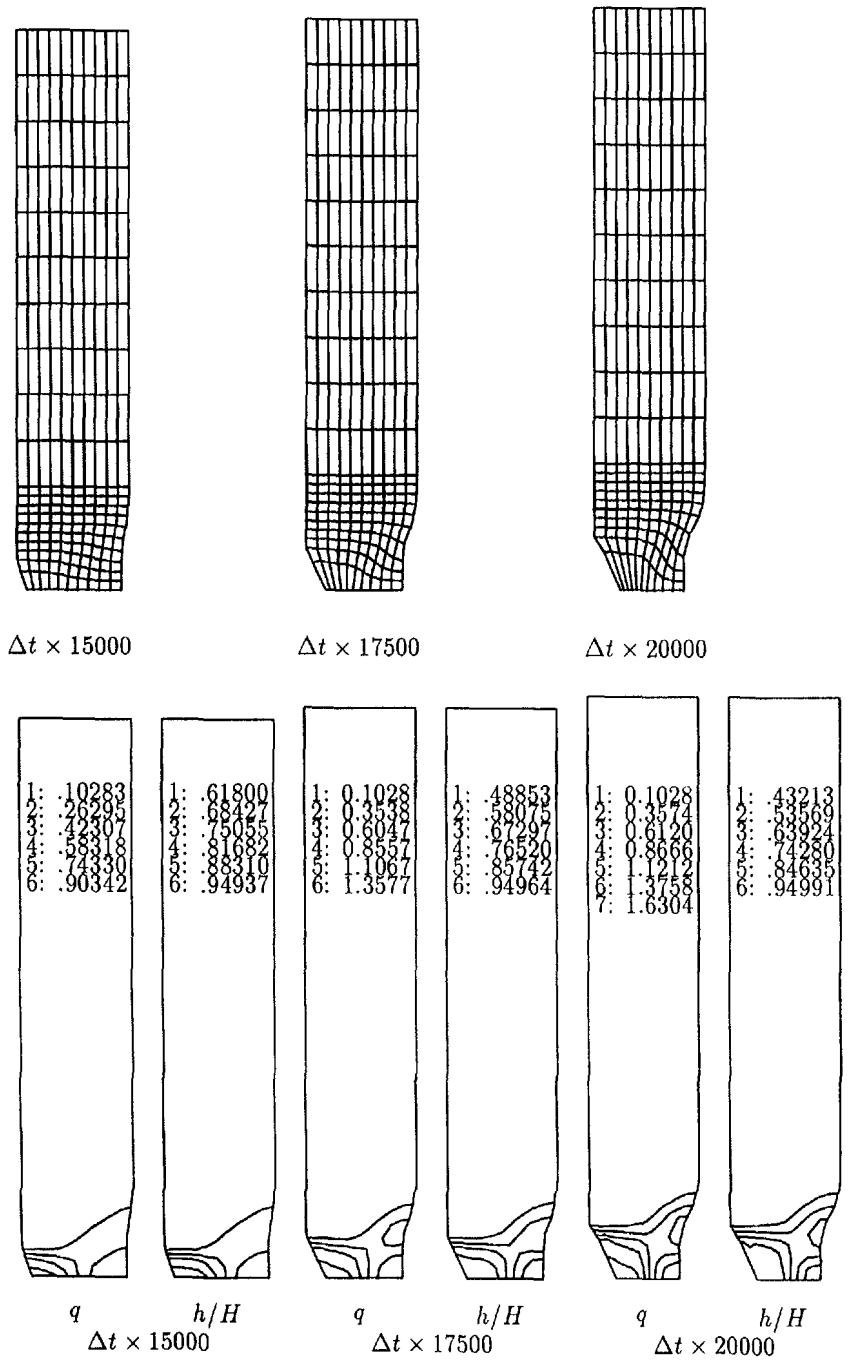

Fig. 2. Dynamic plane stress extension of a thin sheet : case (b).

superposed necking mode tends to diffuse the localized band with ongoing deformation. In contrast the extreme cases (a) and (c) develop pure localization modes which become rather accentuated with increasing elongation.

9. SUMMARY AND CONCLUSION

We presented a formulation of an orthotropic yield condition within the framework of large strain multiplicative elastoplasticity. To this end, the basic assumption is a stress free iso-clinic plastic intermediate configuration with prefered axes of the material described by a three structural tensors combining into one anisotropy tensor. Then an orthotropic yield condition was proposed as an isotropic function of a the Mandel stress in the

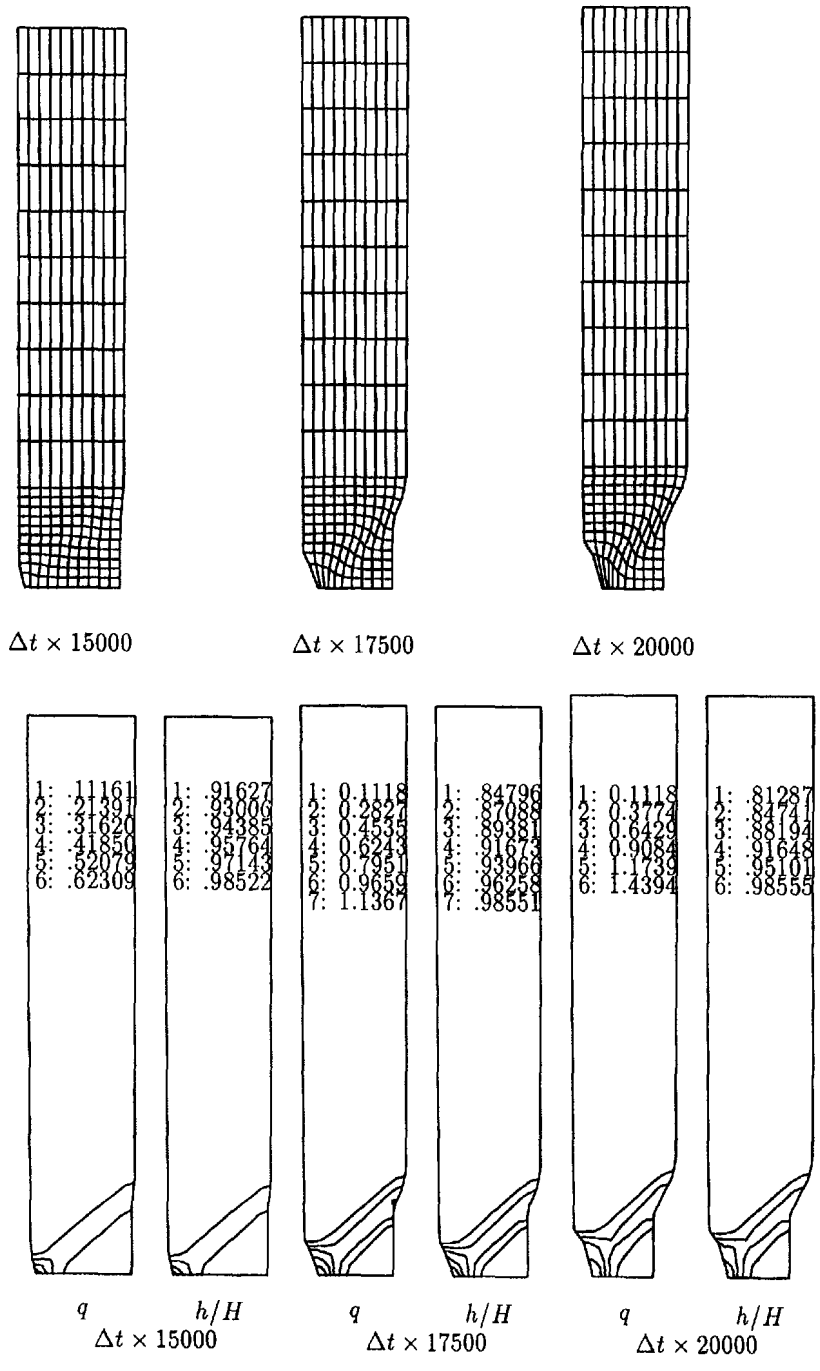

Fig. 3. Dynamic plane stress extension of a thin sheet: case (c).

intermediate configuration and the resulting second order anisotropy tensor. Thereby, we motivated the choice of the invariants in the yield condition by straightforward arguments. In order to concentrate exclusively on the effects related to the orthotropic loading function we assumed the hyperelastic response to be isotropic. For the integration of the flow rule we resorted to the implicit plastic volume preserving exponential map integrator which is easily evaluated due to the restriction to an isotropic elastic response. Concerning the finite element formulation, we described an element technology to recover the plane stress response of 3D constitutive models without any plane stress specific modifications. Thereby, it is possible to show that for thin elements the plane stress constraint is indeed satisfied in the weak sense with the variation of the thickness as weighting function.

Motivated by catastrophic loading cases or metal forming where high speed deformations of thin metal sheets are very likely to occur we invoked an explicit time stepping algorithm designed to handle the developed plane stress element. In the numerical simulation we examined the plane stress extension of a thin metal sheet and studied the influence of orthotropy in the yield strength on the resulting failure patterns. The interesting observation of this numerical study is the intriguing influence of the orthotropic yield condition on the resulting spatial orientation of localized failure modes which emerge under the plane stress constraint in the large strain regime. As extreme cases we detected on the one hand a brittle splitting tension type mode and on the other hand the ductile shear banding mode which is well known from plane strain calculations incorporating the isotropic von Mises model.

As a conclusion it is believed that this contribution clarified the formulation and numerical treatment of an orthotropic yield condition and that the numerical study highlighted the enormous interrelation between the degree of transverse isotropy and the failure patterns of flat metal sheets under uniaxial extension.

Acknowledgement—The authors like to acknowledge the support of this research by the Deutsche Forschungsgemeinschaft under the grant STE 238/25-5.

REFERENCES

Asaro R. J. (1983). Crystal plasticity. *J. Appl. Mech. (ASME)* **50,** 921–934.
Betsch P., Gruttmann F. and Stein E. (1995). A 4-node finite shell element for the implementation of general hyperelastic 3D-elasticity at finite strains. *Comp. Meth. Appl. Mech. Engng* (in press).
Büchter N., Ramm E. and Roehl D. (1994). Three-dimensional extension of non-linear shell formulations based on the enhanced assumed strain concept. *Int. J. Num. Meth. Engng* **37,** 2551–2568.
Boehler J. P. (1987). *Applications of Tensor Functions in Solid Mechanics*. Springer-Verlag, Wien.
Borst R. de and Feenstra P. H. (1990). Studies in anisotropic plasticity with reference to the Hill criterion. *Int. J. Num. Meth. Engng* **29,** 315–336.
Hill R. (1948). A theory of the yielding and plastic flow of anisotropic materials. *Proc. Roy. Soc., A* **193,** 281–297.
Hill R. (1950). *The Mathematical Theory of Plasticity*. Clarendon Press, Oxford.
Hughes T. J. R. (1987). *The Finite Element Method*. Prentice Hall, Englewood Cliffs, New Jersey.
Lee E. H. (1969). Elastic-plastic deformations at finite strains. *J. Appl. Mech. (ASME)* **36,** 1–6.
Lubarda V. A. (1994). An analysis of large strain damage elastoplasticity. *Int. J. Solids Structures* **31,** 2951–2964.
Lubliner J. (1984). A maximum-dissipation principle in generalized plasticity. *Acta Mech.* **52,** 225–237.
Lubliner J. (1986). Normality rules in large-deformation plasticity. *Mech. Mat.* **5,** 29–34.
Mandel J. (1966). Conditions de stabilité et postulat de Drucker. In *Rheology and Soil Mechanics* (Edited by J. Kravtchenko and P. M. Sirieys). Springer-Verlag, Berlin.
Mandel J. (1972). Plasticité classique et viscoplasticité. *Cours au CISM No.* 97, *Udine* '71. Springer-Verlag, Berlin.
Mathur K. K., Needleman A. and Tvergaard V. (1994). Ductile failure analyses on massively parallel computers. *Comp. Meth. Appl. Mech. Engng* **119,** 283–309.
Miehe C. and Stein E. (1992). A canonical model of multiplicative elasto-plasticity. Formulation and aspects of the numerical implementation. *Eur. J. Mech. A/Solids* **11,** 25–43.
Miehe C., Stein E. and Wagner W. (1994). Associative multiplicative elastoplasticity. Formulation and aspects of the numerical implementation including stability analysis. *Comp. Struct.* **52,** 969–978.
Miehe C. (1994). On the representation of Prandtl–Reuss tensors within the framework of multiplicative elastoplasticity. *Int. J. Plast.* **10,** 609–621.
Miehe C. (1995). Exponential map algorithm for stress updates in anisotropic multiplicative elastoplasticity for single crystals. *Int. J. Num. Meth. Engng* (in press).
Needleman A. and Tvergaard V. (1984). Finite element analysis of localization in plasticity. In *Finite Elements: Special Problems in Solid Mechanics*, Vol. V. Prentice Hall, Englewood Cliffs, New Jersey.
Rice J. R. (1976). The localization of plastic deformation. In *Theoretical and Applied Mechanics* (Edited by W. T. Koiter). North Holland, Amsterdam.
Simo J. C. (1988). A framework for finite strain elastoplasticity based on the maximum plastic dissipation and the multiplicative decomposition: Parts I and II. *Comp. Meth. Appl. Mech. Engng* **66,** 199–219, **68,** 1–31.
Simo J. C. (1992). Algorithms for static and dynamic multiplicative plasticity that preserve the classical return mapping schemes of the infinitesimal theory. *Comp. Meth. Appl. Mech. Engng* **99,** 61–112.
Simo J. C. and Armero F. (1992). Geometrically nonlinear enhanced strain mixed method and the method of incompatible modes. *Int. J. Num. Meth. Engng* **33,** 1413–1449.
Simo J. C. and Miehe C. (1992). Associated coupled thermoplasticity at finite strains: formulation, numerical analysis and implementation. *Comp. Meth. Appl. Mech. Engng* **98,** 41–104.
Simo J. C. and Rifai M. S. (1990). A class of mixed assumed strain methods and the method of incompatible modes. *Int. J. Num. Meth. Engng* **29,** 1595–1638.
Steinmann P. and Willam K. (1991). Performance of enhanced finite element formulations in localized failure computations. *Comp. Meth. Appl. Mech. Engng* **90,** 845–867.
Steinmann P., Miehe C. and Stein E. (1993). Comparison of different finite deformation inelastic damage models within multiplicative elastoplasticity for ductile materials. *Comp. Mech.* **13,** 458–474.

Steinmann P., Miehe C. and Stein E. (1994). On the localization analysis of orthotropic Hill type elastoplastic solids. *J. Phys. Mech. Solids* **42,** 1969–1994.

Steinmann P., Betsch P. and Stein E. (1995). FE plane stress analysis incorporating arbitrary 3D large strain constitutive models. *Engr. Comp.* (submitted).

Taylor R. L., Beresford P. J. and Wilson E. L. (1976). A non-conforming element for stress analysis. *Int. J. Num. Meth. Engng* **10,** 1211–1219.

Tvergaard V., Needleman A. and Lo K. K. (1981). Flow localization in the plane strain tensile test. *J. Mech. Phys. Solids* **29,** 115–142.

APPENDIX A

In the coordinate system given by the axes of orthotropy $\mathbf{N}^I$ we may sample the stresses in vector form and recast the deviatoric anisotropy tensor in a matrix $\mathbf{P}$ as

$$\mathbf{P}=\frac{1}{9}\begin{bmatrix} 4a_1^2+a_2^2+a_3^2 & a_3^2-2a_1^2-2a_2^2 & a_2^2-2a_1^2-2a_3^2 & 0 & 0 & 0 \\ a_3^2-2a_1^2-2a_2^2 & a_1^2+4a_2^2+a_3^2 & a_1^2-2a_2^2-2a_3^2 & 0 & 0 & 0 \\ a_2^2-2a_1^2-2a_3^2 & a_1^2-2a_2^2-2a_3^2 & a_1^2+a_2^2+4a_3^2 & 0 & 0 & 0 \\ 0 & 0 & 0 & 18a_1a_2 & 0 & 0 \\ 0 & 0 & 0 & 0 & 18a_2a_3 & 0 \\ 0 & 0 & 0 & 0 & 0 & 18a_3a_1 \end{bmatrix}. \tag{A1}$$

APPENDIX B

From uniaxial yield stresses $S_{(II)}=Y_{(II)}$ applied in the $\mathbf{N}^I$ directions, respectively, we obtain the constants in $\mathbf{a}$ related to the uniaxial yield stresses in the axes of orthotropy

$$\begin{bmatrix} 4 & 1 & 1 \\ 1 & 4 & 1 \\ 1 & 1 & 4 \end{bmatrix}\begin{bmatrix} a_1^2 \\ a_2^2 \\ a_3^2 \end{bmatrix}=6\begin{bmatrix} Y^2/Y_{11}^2 \\ Y^2/Y_{22}^2 \\ Y^2/Y_{33}^2 \end{bmatrix}\rightsquigarrow\begin{bmatrix} a_1^2 \\ a_2^2 \\ a_3^2 \end{bmatrix}=\frac{1}{3}\begin{bmatrix} 5 & -1 & -1 \\ -1 & 5 & -1 \\ -1 & -1 & 5 \end{bmatrix}\begin{bmatrix} Y^2/Y_{11}^2 \\ Y^2/Y_{22}^2 \\ Y^2/Y_{33}^2 \end{bmatrix}. \tag{B1}$$

Clearly, this formulation is closely related to the orthotropic Hill (1948) yield criterion

$$\Phi=\frac{\beta_{12}}{6}[S_{11}-S_{22}]^2+\frac{\beta_{23}}{6}[S_{22}-S_{33}]^2+\frac{\beta_{31}}{6}[S_{33}-S_{11}]^2+\beta_{33}S_{12}^2+\beta_{11}S_{23}^2+\beta_{22}S_{31}^2-\tfrac{1}{3}Y^2=0 \tag{B2}$$

which is usually expanded in terms of the dimensionless parameters β_{IJ} where

$$\beta_{IJ}=\frac{Y^2}{Y_{(II)}^2}+\frac{Y^2}{Y_{(JJ)}^2}-\frac{Y^2}{Y_{(KK)}^2}\quad\text{and}\quad\beta_{(KK)}=\frac{Y^2}{3Y_{IJ}^2}\quad\text{with}\quad\text{I, J, K}\quad\text{cyclic permutation.} \tag{B3}$$

Thereby, the following relations between the Hill representation and the current formulation are easily established

$$\begin{bmatrix} 2 & 2 & -1 \\ 2 & -1 & 2 \\ -1 & 2 & 2 \end{bmatrix}\begin{bmatrix} a_1^2 \\ a_2^2 \\ a_3^2 \end{bmatrix}=3\begin{bmatrix} \beta_{12} \\ \beta_{31} \\ \beta_{23} \end{bmatrix}\rightsquigarrow\begin{bmatrix} a_1^2 \\ a_2^2 \\ a_3^2 \end{bmatrix}=\frac{1}{3}\begin{bmatrix} 2 & 2 & -1 \\ 2 & -1 & 2 \\ -1 & 2 & 2 \end{bmatrix}\begin{bmatrix} \beta_{12} \\ \beta_{31} \\ \beta_{23} \end{bmatrix}. \tag{B4}$$

Nevertheless, the ultimate shear stresses Y_{IJ} in our formulation can not be chosen independently in contrast to the original proposal by Hill since the present formulation introduces the constraints

$$3\beta_{33}=\frac{Y^2}{Y_{12}^2}\doteq 3a_1a_2\quad 3\beta_{11}=\frac{Y^2}{Y_{23}^2}\doteq 3a_2a_3\quad 3\beta_{22}=\frac{Y^2}{Y_{31}^2}\doteq 3a_3a_1. \tag{B5}$$

From the viewpoint of parameter identification, a minimum number of parameters, three in the present proposal in contrast to six in the original Hill (1948) criterion, seems to be advantagous, on the other hand the six parameter formulation allows for a somewhat more involved material behaviour where the ultimate shear strengths are completely independent of the uniaxial yield stresses. In this work we adopt the first viewpoint, since three parameters prove to be sufficient to model orthotropy. Finally, the isotropic von Mises yield condition is recovered by setting $a_I=1$ or equivalently $\beta_{IJ}=1$.

APPENDIX C

For the implementation of the integration algorithm the iteration operator is recast in a matrix format. Thereby, the most involved part reads

$$\mathscr{P}\cdot\mathbf{C}_e+\mathbf{C}_e\cdot\mathscr{P}=\mathscr{A}\cdot\mathbf{C}_e+\mathbf{C}_e\cdot\mathscr{A}-\tfrac{2}{3}[\mathbf{C}_e\otimes\mathbf{A}^2+[\mathbf{C}_e\cdot\mathbf{A}^2]^{\mathrm{sym}}\otimes\mathbf{I}]+\tfrac{2}{9}I_2^{\mathrm{am}}\mathbf{C}_e\otimes\mathbf{I}. \tag{C1}$$

Here we considered only the contributions of $\mathscr{P}$ which act on deviatoric components of $\mathbf{S}$. The matrix representation $\bar{\mathbf{P}}$ of this expression is given in terms of the dimensionless parameters β_{IJ} and the components C^e_{IJ} of $\mathbf{C}_e$ in the coordinate system $\mathbf{N}^I$ as

$$\bar{\mathbf{P}}=\begin{bmatrix}\bar{\mathbf{P}}_a & \bar{\mathbf{P}}_b\\ \bar{\mathbf{P}}_c & \bar{\mathbf{P}}_d\end{bmatrix} \tag{C2}$$

with partitions

$$\bar{\mathbf{P}}_a=\frac{2}{3}\begin{bmatrix}[\beta_{12}+\beta_{31}]C^e_{11} & -\beta_{12}C^e_{11} & -\beta_{31}C^e_{11}\\ -\beta_{12}C^e_{22} & [\beta_{23}+\beta_{12}]C^e_{22} & -\beta_{23}C^e_{22}\\ -\beta_{31}C^e_{33} & -\beta_{23}C^e_{33} & [\beta_{31}+\beta_{23}]C^e_{33}\end{bmatrix} \tag{C3}$$

$$\bar{\mathbf{P}}_b=4\begin{bmatrix}\beta_{33}C^e_{12} & 0 & \beta_{22}C^e_{13}\\ \beta_{33}C^e_{12} & \beta_{11}C^e_{23} & 0\\ 0 & \beta_{11}C^e_{23} & \beta_{22}C^e_{13}\end{bmatrix} \tag{C4}$$

$$\bar{\mathbf{P}}_c=\frac{1}{6}\begin{bmatrix}[\beta_{23}-2\beta_{12}]C^e_{12} & 2\beta_{23}C^e_{12} & -2[\beta_{31}+\beta_{23}]C^e_{12}\\ -2[\beta_{12}+\beta_{31}]C^e_{23} & [\beta_{31}-2\beta_{23}]C^e_{23} & 2\beta_{31}C^e_{23}\\ 2\beta_{12}C^e_{13} & -2[\beta_{23}+\beta_{12}]C^e_{13} & [\beta_{12}-2\beta_{31}]C^e_{13}\end{bmatrix} \tag{C5}$$

$$\bar{\mathbf{P}}_d=2\begin{bmatrix}\beta_{33}[C^e_{11}+C^e_{22}] & \beta_{11}C^e_{13} & \beta_{22}C^e_{23}\\ \beta_{33}C^e_{13} & \beta_{11}[C^e_{22}+C^e_{33}] & \beta_{22}C^e_{12}\\ \beta_{33}C^e_{23} & \beta_{11}C^e_{12} & \beta_{22}[C^e_{33}+C^e_{11}]\end{bmatrix}. \tag{C6}$$

All other parts of the iteration operator are not critical to establish and are therefore omitted.